Journal of Science and Inclusive Development Vol. 5, No. 2, DOI:10.20372/jsid/2023-256

A comparative study on modelling and performances of modular converter based three phase inverters for smart transformer application

Yalisho Girma[1*], Getachew Biru[2] and Chandra Sekhar [1]

[1]Electrical Power and Control Engineering Department, Adama Science and Technology University, Ethiopia

[2]Addis Ababa Institute of Technology (AAiT), AAU, Ethiopia

[*] Corresponding author email: yalisho.girma@gmail.com; https://orcid.org/0000-0003-4390-5670

Received: 28 March 2023; Revised: 19 June 2023; Accepted: 05 November 2023

Abstract

In this paper, the performance evaluation of a three-phase back-end converter (BEC) of a smart transformer using different modular converters and interleaved multi-carrier phase shift modulation techniques was made. The modular backend converter of the smart transformer feeding a 0.415 kV low voltage distribution system and having a capacity of 50 kVA was designed, modelled, and simulated. Different scenarios were used for critically evaluating the performances of the system and included changes in the modulation index (Mi), changes in frequency, load demand changes, and losses. Performance indicators such as the output voltage and current distortions (THD), the maximum current through and voltage across the sub-modules, changes in the output voltage and current magnitude, and converter efficiency are used for the evaluation of different BEC topologies. The Piecewise Linear Electrical Circuit Simulation (PLECS) platform is used to model and simulate the circuits in question. When comparing MMC and CHB-based back-end converters having the same number of converter cells, load type, modulation index, output voltage, and current, the results show that the MMC performs better with respect to THD and efficiency. Regarding efficiency, the converter made from SiC MOSFET with part number SCT3017AL yields a higher efficiency (96.63%) than the second SiC MOSFET with part number C3M0015065D. According to semiconductor loss analysis, switching loss outweighs conduction loss. The sub-module in a CHB-based modular converter is exposed to higher current stress in comparison with that used in an MMC topology due to the current division in the upper and lower sub-modules in the case of MMC. As the load demand changes, the device current value also changes, while the voltage remains constant.

Keywords: Distribution System, Smart Transformer, Modular Converter (MC), Interleaved PWM

List of Abbreviations and Acronyms

BEC	Back End Converter
CHB	Cascaded H-Bridge
LS-PWM	Level Shift Pulse Width Modulation
MMC	Modular Multilevel Converter
FBSM	Full Bridge Sub-Module
HBSM	Half-Bridge Sub-Module
PS-PWM	Phase Shift Pulse Width Modulation
RES	Renewable Energy Source
ST	Smart Transformer
VSI	Voltage Source Inverter
NPC	Neutral Point Clamped
FRD	Fast Recovery Diode
SM	Sub-Module
SVM	Space Vector Modulation
PEBB	Power Electronic Building Block
PLECS	Piecewise Linear Electronics Circuit Systems

Introduction

At present, the electric distribution system is constantly changing in its configuration because of the prevalent utilization of renewable energy sources (RES) and hybrid microgrids with modern distributed energy infrastructures. The conventional low frequency distribution transformer is highly challenged by the extra requirements of present-day distribution systems (Kumar et al., 2017). These extra requirements of today's distribution system include bidirectional power and data flow, easy connection to distributed energy resources, energy storage, load compensation, and improved power quality and reliability.

A smart transformer (ST) can be taken as a competent choice to link AC and DC systems running at medium and low voltage levels. The three-stage smart transformer is among many configurations of smart transformers that fulfil all the extra functionalities demanded by modern distribution systems (Hrishikesan et al., 2020). The back-End converter of the smart transformer (ST) is a voltage source inverter (VSI) interfaced to a low voltage (LV) power distribution system or loads. It converts a low DC link voltage at the output of the DC-DC stage to a sinusoidal AC voltage of 220 V (P-N) or 415 V (L-L), 50Hz specification. Because this stage is frequently vulnerable to LV grid disturbances, a careful design of its output filters (common

Journal of Science and Inclusive Development Vol. 5, No. 2, DOI:10.20372/jsid/2023-256

mode and differential mode filters) is required. The use of mature converter topologies with readily available semiconductors having low blocking voltages (1.2 kV, 1.7kV, 3.3kV) is a well-established and industrially accepted way for converting conventional grid voltage. This stage suffers from the challenges of high current and EMI filter design. In order to handle the high current demand, PWM with an interleaved approach can be used. The design of EMI filters should be carried out with great care to minimize the injection of a high-frequency disturbance into the input source side (Mahammad et al, 2020).

The availability of the neutral conductor is another requirement of this ST stage because the low voltage distribution network is based on the configuration of Terra-Terra (TT). Furthermore, this stage is also exposed to load unbalancing and non-linearity, which creates zero-sequence current that must be properly handled by the three-phase three wire or three-phase four-wire voltage source inverter (VSI). But the four-wire VSI is the most appropriate one with regard to freedom and control of neutral current. Topologies that are most appropriate for the back-end converter stage include a typical two-level voltage source inverter (VSI), a three-level neutral point clamp (NPC), and T-type topologies (Hannan et al., 2020).

However, the conventional two- and three-level voltage source inverters used in low voltage systems suffer from high conduction loss, switching (turn-on and turn-off) loss, and high dV/dt stress because of their high-frequency operation requirements. For developing highly efficient inverters, CHB and MMC-based modular inverters with low switching frequency operation are the focus of this study. Although CHB and MMC-based modular converters have more parts than a non-modular solution, they have many advantages over other topologies (Muhammad et al., 2022; Mikkili et al., 2022; Costa et al., 2017). These advantages include cell and phase modularity, simple voltage and power scaling by combing identical cells, the possibility of using a single capacitor as a means of energy storage for modules, easy bypass of faulty cells during faults (fault ride-through capability), low dV/dt, reduced electromagnetic interference (EMI), cost effectiveness, good transient response, and the possibility of using readily available low voltage power switches.

A literature survey shows that different PWM techniques have been discussed for operating a BEC (Marcelo et al., 2021; Jayakuma and Vanitha, 2019). Sub-module capacitor voltage unbalancing is a common problem in BEC. Assessment of studies so far done on multilevel inverters has focused on the impact of different levels of CHB and MMC on increasing the quality of power systems without specifically comparing the performance of two types of modular inverters with respect to converter efficiency, voltage THD, and device current stress.

The design and comparative performance evaluation of CHB and MMC-based nine-level back-end converters applied to 0.415kV; 50kVA low voltage distribution system will be the focus of this study.

The rest of the paper's content is structured as follows: Section 2 reviews the configurations of modular BEC. The basic working principles and mathematical approach to analysing the power circuit operation of the back-end converter (BEC) are treated in Section 3. Section four discusses different multicarrier PWM techniques. Simulation results and performance comparisons of CHB and MMC-based nine (9)-level back-end converter configurations for different scenarios are made in Section 5. The last part of the paper concludes the work.

Research methodology

This research used a simulation method to evaluate the performances of the two types of modular multilevel backend converters for smart transformers. The power circuit and modulation circuit of both CHB and MMC-based modular converters are modelled in the Simulink/PLECS simulation package, and their performance is evaluated for different scenarios such as changes in load demand, changes in the modulation index, and changes in the modulation frequency. Performance indicators such as output voltage distortions, current THD, efficiency (loss), and sub-module current stress are used for evaluation and comparison.

Configuration of modular converter

The two-level and three-level VSI suffer from high dV/dt and di/dt and lack intelligent operation (activation and deactivation of modules) during partial loading of the distribution grid. A possible solution to these problems is to use different types of multilevel inverters that utilise low-voltage switches and low switching frequencies, as discussed in Zhang et al. (2012). The CHB and MMC shown in Figures 1 and 2 are proposed modular back-end converters for low-voltage distribution systems. The basic building block of a CHB-based modular backend converter is the full bridge sub-module, made of four power electronic switches connected in an H-bridge shape, as shown in Figure 3(b). One of the drawbacks of the CHB-based modular BEC is that it uses a separate voltage source for each sub-module. For the MMC-based modular BEC, many topologies can be used as basic building blocks, but the half-bridge sub-module shown in Figure 3 (a) is selected as it has a low switch count and hence low switching and conduction losses.

Journal of Science and Inclusive Development Vol. 5, No. 2, DOI:10.20372/jsid/2023-256

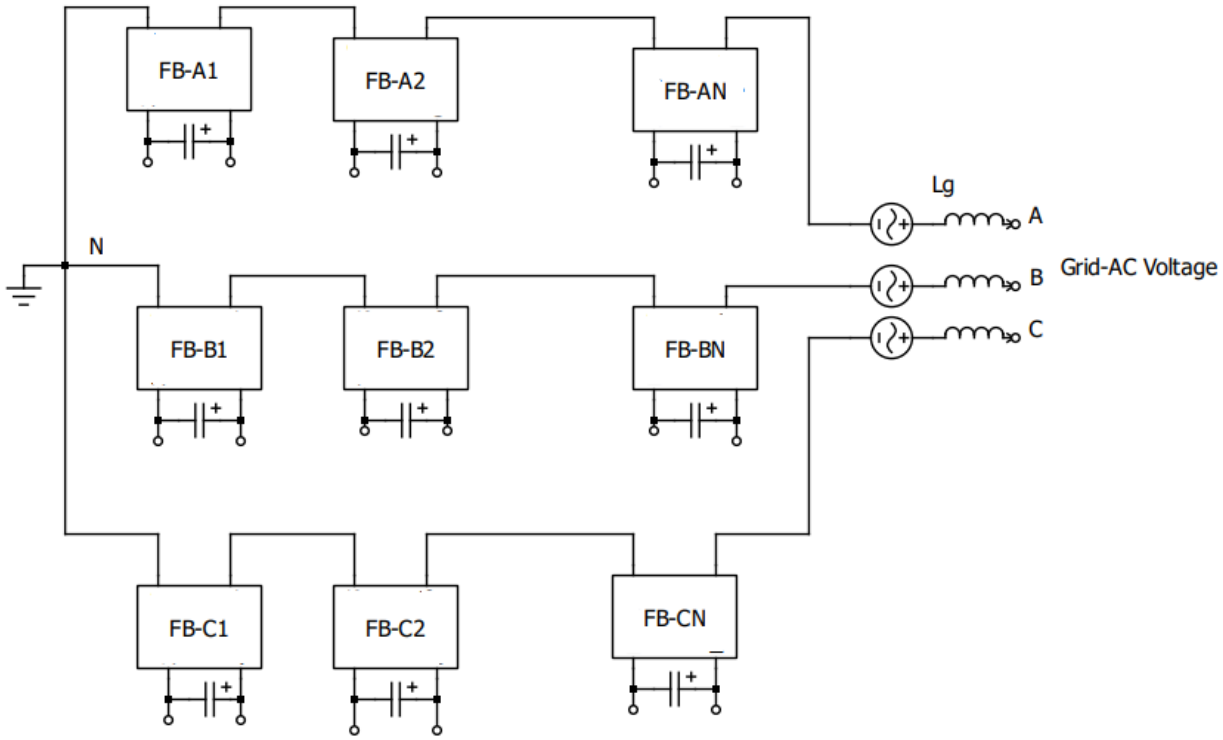

Figure1. CHB based modular converter

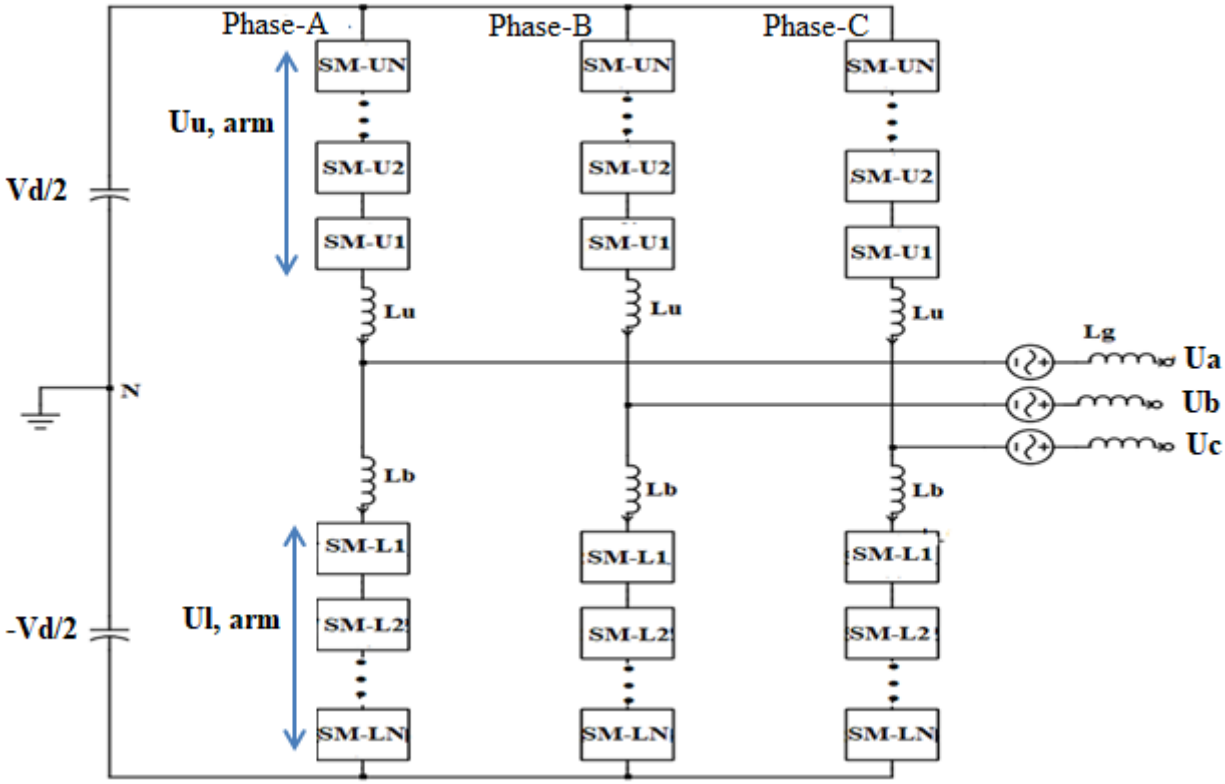

Figure 2. MMC based modular converter

Design and analysis of modular converter

For the design of a back-end converter, issues such as converter building block, output voltage magnitude and quality, input DC magnitude, and load type to be served should be taken into consideration. With respect to power electronic building blocks (PEBB), half bridges (HB) and full bridges (FB) utilizing IGBT or MOSFET technology, as shown in Figure 3, can be used in the modelling of the back-end converter of a smart transformer.

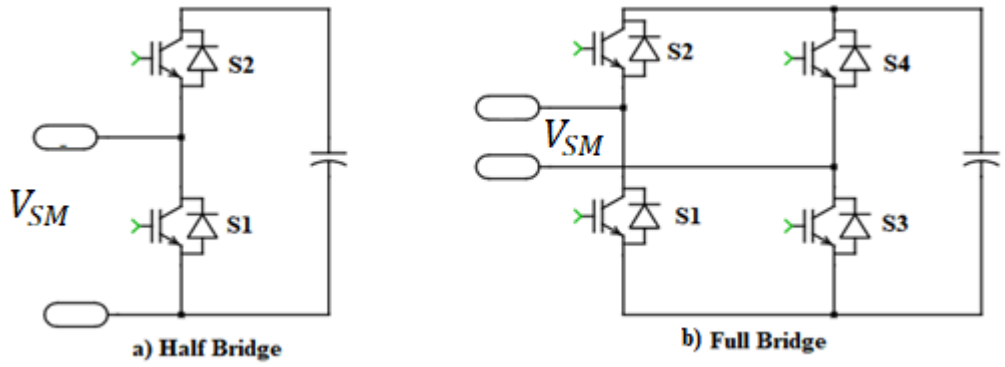

Figure 3. Converter basic building block

The half-bridge IGBT/MOSFET power sub-module from which MMC is built is operating in complementary mode, and depending on the states of the upper and lower switches and current direction, the sub-module can be in one of four states described in Figure 4.

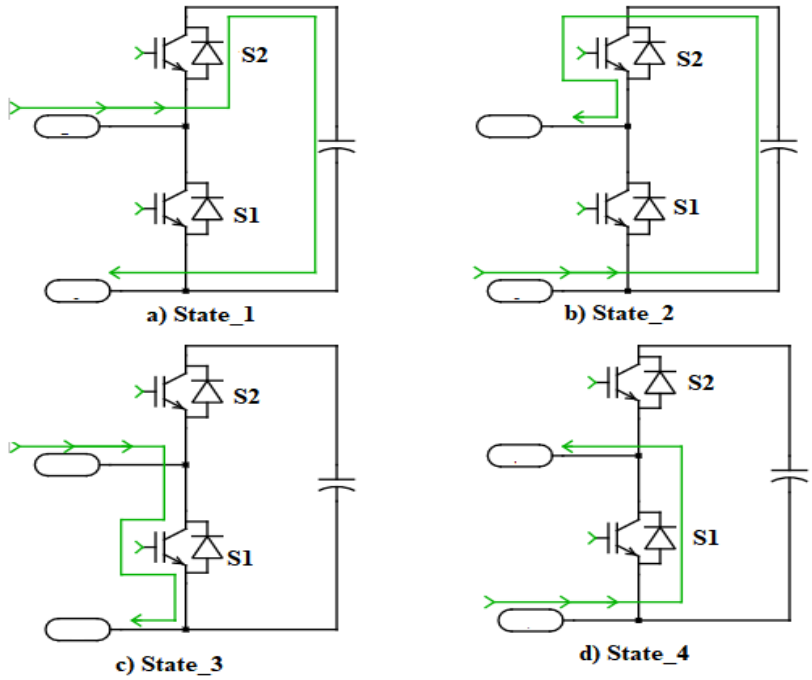

Figure 4. Half- bridge switch transition states

Journal of Science and Inclusive Development Vol. 5, No. 2, DOI:10.20372/jsid/2023-256

As shown in Figure 4, when the sub-module (SM) is in state one, the SM capacitor is inserted and charged through the upper clamping diode, giving the SM voltage equal to the capacitor voltage. When the SM is in state two, its capacitor is inserted and discharging through the upper IGBT/MOSFET, making the SM voltage equal to the capacitor voltage. When the SM is either in state three or state four, its capacitor is bypassed, hence the SM voltage equals zero.

The full bridge sub-module (FBSM) shown in Figure 3 (b) has three output voltages depending on four switch states, namely, -VSM, 0V, and VSM. As a result, the AC output phase voltage waveform for a CHB-based inverter is composed of 2N + 1 levels given by the sum of the sub-module voltages, as shown below (Pierluigi et al., 2016).

$$V_{inv} = \sum_{i}^{N} H_j \;\; V_{SMi} \qquad (1)$$

Where H_j is modulation factor with j= -1, 0, 1 and V_{SMi} is the DC voltage of SM.

In the same way, the half bridge sub-module (HBSM) in the upper arm and lower arm of the MMC leg can have –VSM, 0 and +VSM and for N number of sub-modules in the leg arm, equation (1) holds true for the inverter output voltage of an MMC-based inverter. The relation between input dc voltage, upper arm voltage, and output inverter voltage per phase for a controlled MMC-based inverter shown in Figure 2 can be given by the following equation:

$$U_{a_{(\max)}} \cos(\omega t) = \frac{V_d}{2} - \mathrm{Uu,arm} \quad (2)$$

where is the sum of N upper arm sub-modules (Arvind, 2019; Pierluigi et al., 2016).

The power electronic building block used to implement a back-end converter is selected based on the type of application and maximum load current and voltage requirements. Based on the power distribution system specification, the maximum load current is 72 A, and line-to-line AC voltage is 415 V with a lagging power factor ranging from 0.95 to 1. Therefore, IGBTs /MOSFET having a blocking voltage rating of 200 V or greater and a current rating of 80 A or greater will be considered by device manufacturers such as CREE, Infineon, and ROHM. A sufficient safety factor of two (2) is used to derate the device ratings so that operation in the transient condition is safe. Nine levels (9-level) back-end converters based on CHB and MMC topologies are considered for this project.

After evaluation of the semiconductor device manufacturer’s data sheet, the following semiconductor power switches, explained in Table 1, are chosen for design and simulation purposes:

Table 1. Chosen semiconductor power switches for system

Device part number	Voltage rating (V)	Current rating(A) @100^{0}C	Manufacturer
SiC-power MOSFET (SCT3017AL)	650	83	RHOM
SiC-Power MOSFET (C3M0015065D)	650	96	CREE

For analysis of the three-phase backend converter of a smart transformer based on MMC, a single-phase equivalent circuit illustrated in Figure 5 below is derived from Figure 2.

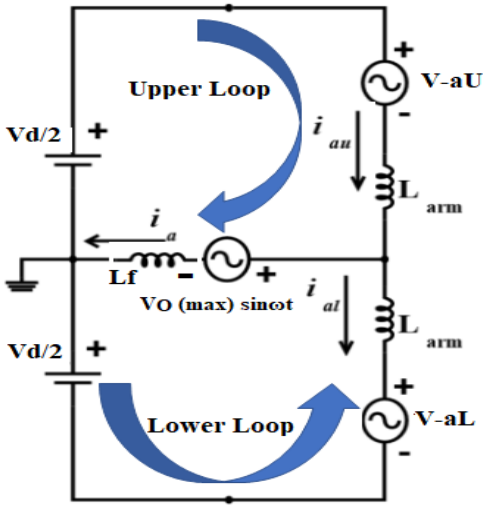

Figure 5. Single phase equivalent circuit of MMC

Based on the equivalent circuit in Figure 5, the currents through switches and diodes in the upper and lower arms of the phase leg are given as follows (Subhadeep et al., 2013).

$$I_{av\,US} = \frac{1}{2\pi}\left(mI_{dc}\cos\alpha - \frac{1}{2}I_{pp}\right) \quad (3)$$

$$I_{av\,UD} = -\frac{1}{2\pi}\left(mI_{dc}\cos\alpha - \frac{1}{2}I_{pp}\right) \quad (4)$$

$$I_{av\,LS} = \frac{1}{2}I_{dc} + \frac{1}{2\pi}\left(mI_{dc}\cos\alpha + \frac{1}{2}I_{pp}\right) \quad (5)$$

$$I_{av\,LD} = \frac{1}{2}I_{dc} - \frac{1}{2\pi}\left(mI_{dc}\cos\alpha + \frac{1}{2}I_{pp}\right) \quad (6)$$

$$I_{rms\,US}{}^2 = \frac{1}{2\pi}\left[\frac{1}{2}\left(\frac{1}{8}I_{pp}{}^2 - I_{dc}{}^2\right) - \frac{5}{6}I_{dc}I_{pp} + m\cos\alpha\left(I_{dc}{}^2 + \frac{1}{8}I_{pp}{}^2\right)\right] \quad (7)$$

Journal of Science and Inclusive Development Vol. 5, No. 2, DOI:10.20372/jsid/2023-256

$$I_{rms\,UD}{}^2 = \frac{1}{2\pi}\left[\frac{1}{2}\left(\frac{1}{8}I_{pp}{}^2 - I_{dc}{}^2\right) + \frac{5}{6}I_{dc}I_{pp} - m\cos\alpha\left(I_{dc}{}^2 + \frac{1}{8}I_{pp}{}^2\right)\right] \quad (8)$$

$$I_{rms\,LS}{}^2 = \frac{1}{2\pi}\left[\frac{1}{2}\left(\frac{1}{8}I_{pp}{}^2 + 3I_{dc}{}^2\right) + I_{dc}I_{pp} + m\cos\alpha\left(I_{dc}{}^2 + \frac{1}{6}I_{pp}{}^2\right)\right] \quad (9)$$

$$I_{rms\,LD}{}^2 = \frac{1}{2\pi}\left[\frac{1}{2}\left(\frac{1}{8}I_{pp}{}^2 + 3I_{dc}{}^2\right) - I_{dc}I_{pp} + m\cos\alpha\left(I_{dc}{}^2 + \frac{1}{12}I_{pp}{}^2\right)\right] \quad (10)$$

$$I_{dc} = m\cos\alpha\left(\frac{Ipp}{4}\right) \quad (11)$$

where, m is index of modulation, I_{pp} is phase current peak to peak value, Cosα is load power factor, Idc is the phase leg DC current, $I_{av\,US}$, $I_{av\,LS}$, $I_{av\,UD}$, $I_{av\,LD}$ are the average currents flowing in switches and diodes at upper and lower arm of phase leg.

$I_{rms\,US}$, $I_{rms\,LS}$, $I_{rms\,UD}$ and $I_{rms\,LD}$ are the RMS current values of switch and diode in the upper and lower side respectively.

The input DC power and output AC power can be related by:

$$P_{dc} = V_{dc}I_{dC} = P_{ac} + losses = 0.5m\frac{Vdc}{2}I_{pp}\cos\alpha + Losses \quad (12)$$

The losses produced in power electronic systems are caused by intrinsic components such as power electronic devices and ohmic resistors (stray resistance). Power electronics dissipate losses due to their non-ideal nature. These losses can be grouped into conduction losses, switching losses, and blocking losses. Blocking loss, which is caused by small leakage currents, can be ignored in most analyses without causing much inaccuracy. For power electronic devices integrated with diodes, such as the MOSFET with a fast recovery diode, losses should be individually specified for both the semiconductor switch and diode.

The losses that happen while the MOSFET or fast recovery diode is turned on and conducting current are referred to as conduction losses. Conduction power loss is determined by the product of the on-state voltage and the on-state current. However, multiplying the total conduction loss by the duty factor is a requirement in applications where PWM is used.

The total conduction loss dissipated by the MOSFET integrated with the fast recovery diode is given by the following equation.

$$Pcond(tot) = Pcond(IGBT/MOSFET) + Pcond(Diode) \quad (13)$$

$$Pcond(IGBT/MOSFET) = \frac{1}{T}\int_0^T [V_{CE}(t) * I_C(t)]dt \quad (14)$$

The average conduction loss of IGBT can be computed by the following equation:

$$\text{Pav}(cond) = V_{CE(S)} * I_C * \delta \qquad (15)$$

Where, δ refers to device duty cycle

The transitions of MOSFETs and FRD from on-state to off-state and vice versa do not occur instantly, which results in switching losses. Both the current flowing through and the voltage across the device during the transition interval are remarkably larger than zero, which leads to large instantaneous power losses.

Equations to determine the switching power losses for MOSFETs and FRD are given bellow:

$$\text{Psw}(IGBT/MOSFET) = E_{ON} + E_{OFF} * \quad f_{SW} \qquad (16)$$

$$\text{Psw(FRD)} = \text{E}_{\text{rec}} * \quad \text{f}_{\text{SW}} \qquad (17)$$

The turn-on energy (Eon), the turn-off energy (Eoff) in the IGBT, and the reverse recovery energy in the FRD (Erec) are functions of collector current, collector voltage, gate resistance, and junction temperature.

Normalization of the switching losses with the conditions provided for any application and the nominal values from the datasheet is essential.

$$\text{Psw}(MOSFET) = \left(\frac{E_{ON} + E_{OFF}}{\pi}\right) * f_{SW} * \frac{I_{pk}}{I_{nom}} * \frac{V_{DC-link}}{V_{nom}} \qquad (18)$$

$$\text{Psw}(FWD) = (E\_rec/\pi) * f\_SW * I\_pk/I\_nom * V\_(DC - link)/V\_nom \qquad (19)$$

From the determination of the switching and conduction losses of MOSFET and FRD, it is possible to obtain the total loss for determining the efficiency of the system and the junction temperature of the devices.

$$\text{P}(tot) = P_{Cond}(MOSFET) + P_{SW}(MOSFET) + P_{Cond}(FRD) + P_{SW}(FRD) \qquad (20)$$

Piecewise linear electronics circuit systems (PLECS) use a lookup table, formula, or combination of lookup table and formula approaches to determine conduction and switching losses (Plexim GmbH, 2023). The lookup approach uses interpolation and extrapolation methods to find the device loss values based on the set of data points taken from the datasheet. The novelty of this research work is justified by the integration of device thermal models and efficiency calculation models for converters. A thermal implementation model for a single MOSFET integrated with FRD is given in Figure 6 below. For power electronic systems containing multiple switches, the same approach can be used with a common heat sink shared among all semiconductor switch packages.

Journal of Science and Inclusive Development Vol. 5, No. 2, DOI:10.20372/jsid/2023-256

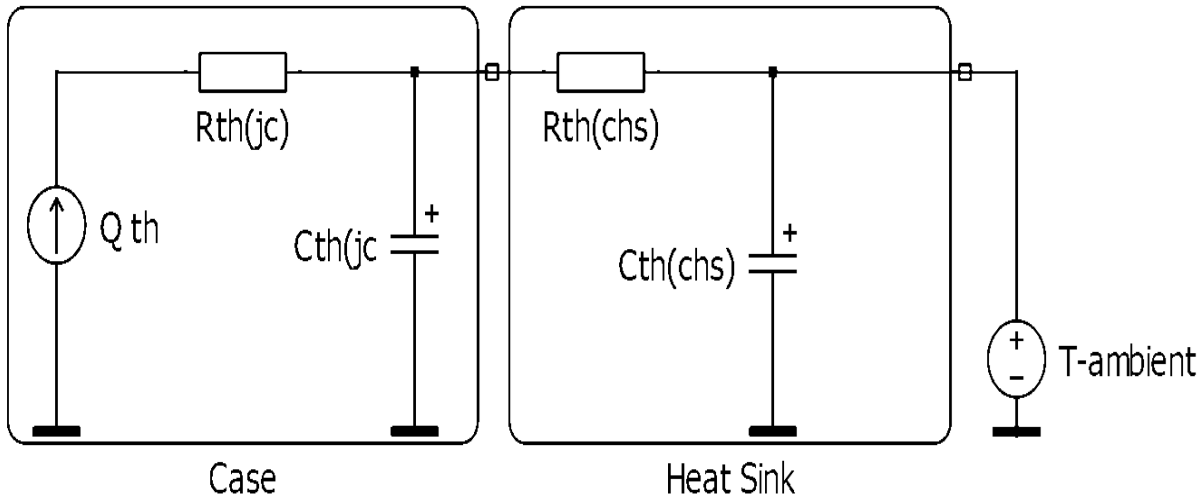

Figure 6. Thermal model of a single semiconductor device

Based on the thermal data collected from the device manufacturer, switching loss and conduction loss models of the selected semiconductor switches are generated, as shown in Figure 7(a to c).

The converter efficiency calculation model described in Figure 8 uses these thermal loss models for the loss and efficiency calculations of the system. The periodic average for conduction losses and the periodic impulse average for switching losses obtained from probe output are summed to get the total converter loss (Plexim GmbH, 2023).

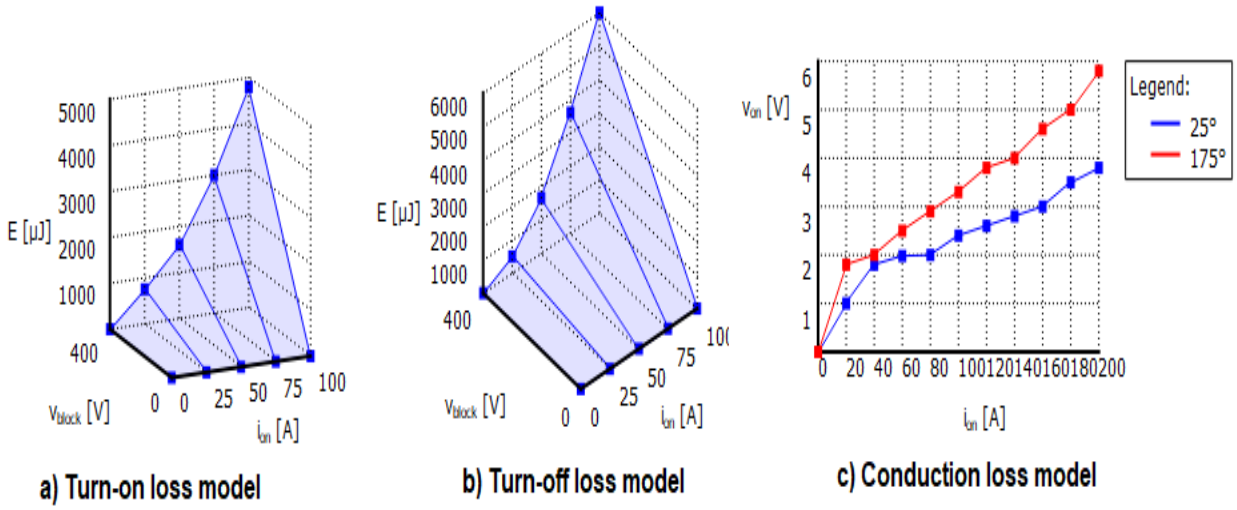

Figure 7. Loss model of MOSFETs with FRD

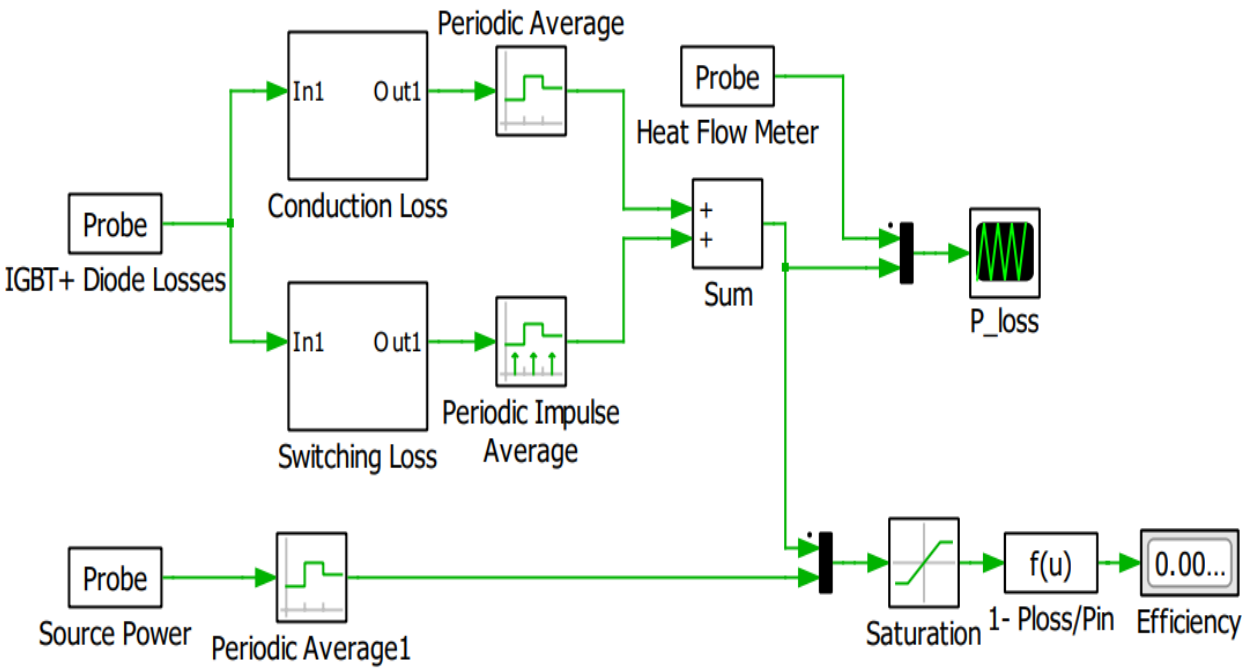

Figure 8. Efficiency calculation model

Modulation strategy

Numerous modulation strategies for the MMCs have been proposed by many researchers, such as nearest level control (NLC), Level Shifted Carrier based PWM, phase shifted pulse width modulation (PSPWM) and space vector modulation (SVM) (Konstantinou et al., 2016).

Due to its ease of use in low-voltage modules and even distribution of the modulation signal in all sub-modules, multi-carrier pulse width modulation strategies are frequently employed for MMC-based modular converters. Multi-Carrier PWM is classified as Phase shifted PWM and level shifted and techniques (Rohner et al., 2010). Level shift PWM creates complexity in the modulation circuit as the number of voltage levels increases, and hence a phase shift modulation is used in this project.

In PS-PWM, the capacitor voltage of SM is balanced with a PI controller, and there is no need to use a sorting algorithm as in LS-PWM. The superior performance of PS-PWM over LS-PWM is revealed when the output voltage is large.

To create the switching signals for a PS-PWM multilevel converter, multiple carriers are needed. Over the course of the switching cycle, multiple carriers exist simultaneously. Typically, a multilevel converter will need as many carriers as there are voltage levels in the output voltage, excluding one. If N is the number of sub-modules in each arm, then the phase difference between the carriers can be found using the equation below (Rohner et al., 2010).

Journal of Science and Inclusive Development Vol. 5, No. 2, DOI:10.20372/jsid/2023-256

$$\theta = 360/N \qquad (21)$$

The time interval between consecutive switching signals is given by the equation below:

$$Td = 1/(N * f_C) \qquad (22)$$

where, f_C is the carrier frequency.

For the implementation of phase-shifted PWM signals, the reference voltage (modulating signal) is compared with a triangular waveform (carrier signal) in a comparator block to determine the switching sequence for the converter.

The comparator block yields a high switching signal (1 = switch ON) when the triangular wave is higher than the reference voltage; otherwise, it yields a low signal (0 =switch OFF). The switches in one leg of HBSM and FBSM operate in a complementary manner to avoid short-circuiting. The PS-PWM signal generation technique inside the comparator block for two sub-modules (N=2) is given by the signal diagram in Figure 9.

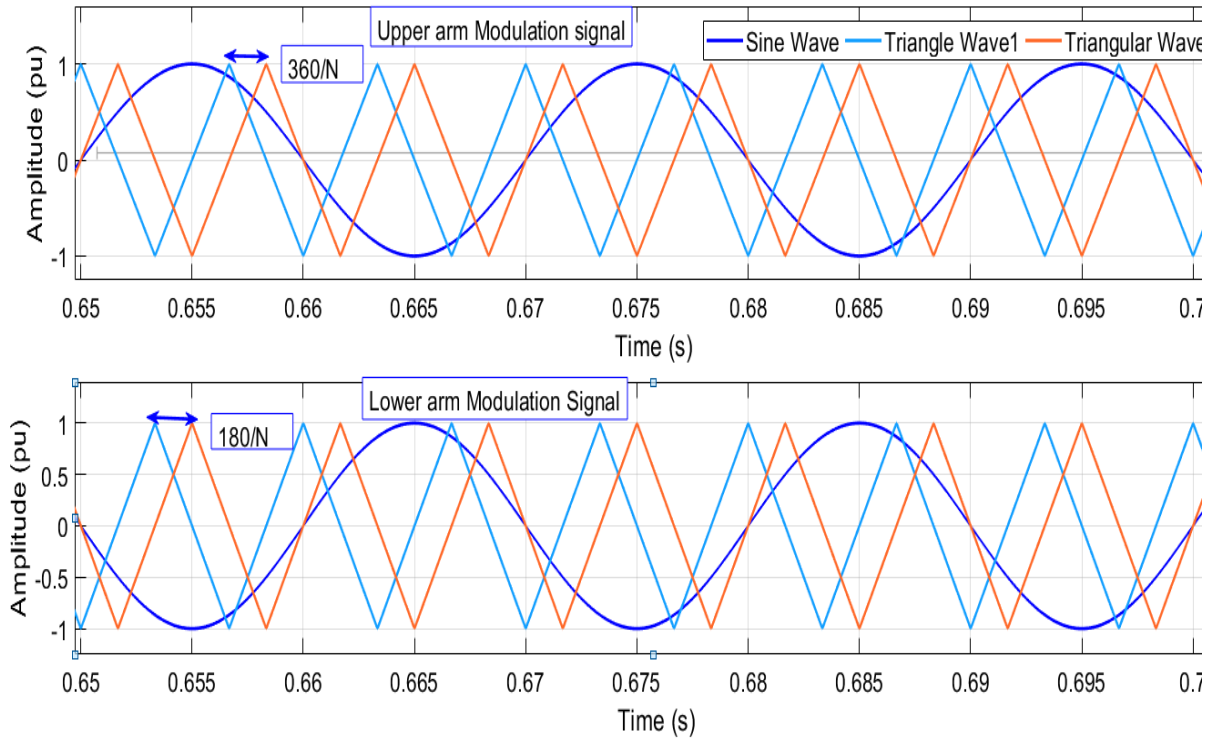

Figure 9. Interleaved phase shift modulation

The use of an MMC-based back-end converter gives a chance to scale up the number of levels in the output voltage by a factor of 2 for the same structure by using interleaved phase shift modulation with π phase angles between the upper and lower arm carriers. This feature of an MMC-based BEC gives an output voltage with better THD values. In order to utilize the above advantage, the interleaved phase modulation technique is applied in this project work.

Simulation result and discussion

For simulating the models of BEC of smart transformers based on CHB and MMC topologies, a three-phase star-connected inductive load (R-L load) with a power factor ranging from 0.9 to 1 and a three-phase diode rectifier as a non-linear load have been used. Both types of loads have a maximum rating of 50kVA. A steady-state system analysis is used to see changes in output voltage and current.

In Table 2, the parameter values of the distribution system and converters are listed. These absolute values were incorporated into the PLECS/Simulink modelling to create the system.

Table 2. Technical design of the System

Parameters	Value
Output AC Line Voltage(Vg)	415V
Output AC side Inductance (Lg)	3.33mH
Output AC side resistance (R_g)	3.33 Ω
Maximum Power(S)	50kVA
Load Power factor	0.95 to 1 lagging
Sub-module arm inductance (L_arm)	3mH
Sub-module arm resistance (R_arm)	0.1 Ω
Sub-module arm capacitance ($C_{\_SM}$)	20mF
Capacitance at DC link ($C_{\_DC\ Link}$)	20mF
Distribution system frequency(f_g)	50Hz
Carrier frequency (f_c)	1000Hz to 8000Hz
Modulation index	1
Type of Modulation	Interleaved Phase shift PWM
DC Voltage	710V for MMC & 85V for CHB cell
No of Sub-module per arm (SM)	4

Journal of Science and Inclusive Development Vol. 5, No. 2, DOI:10.20372/jsid/2023-256

A) Results for CHB based BEC

A.1 Performance for R-L load

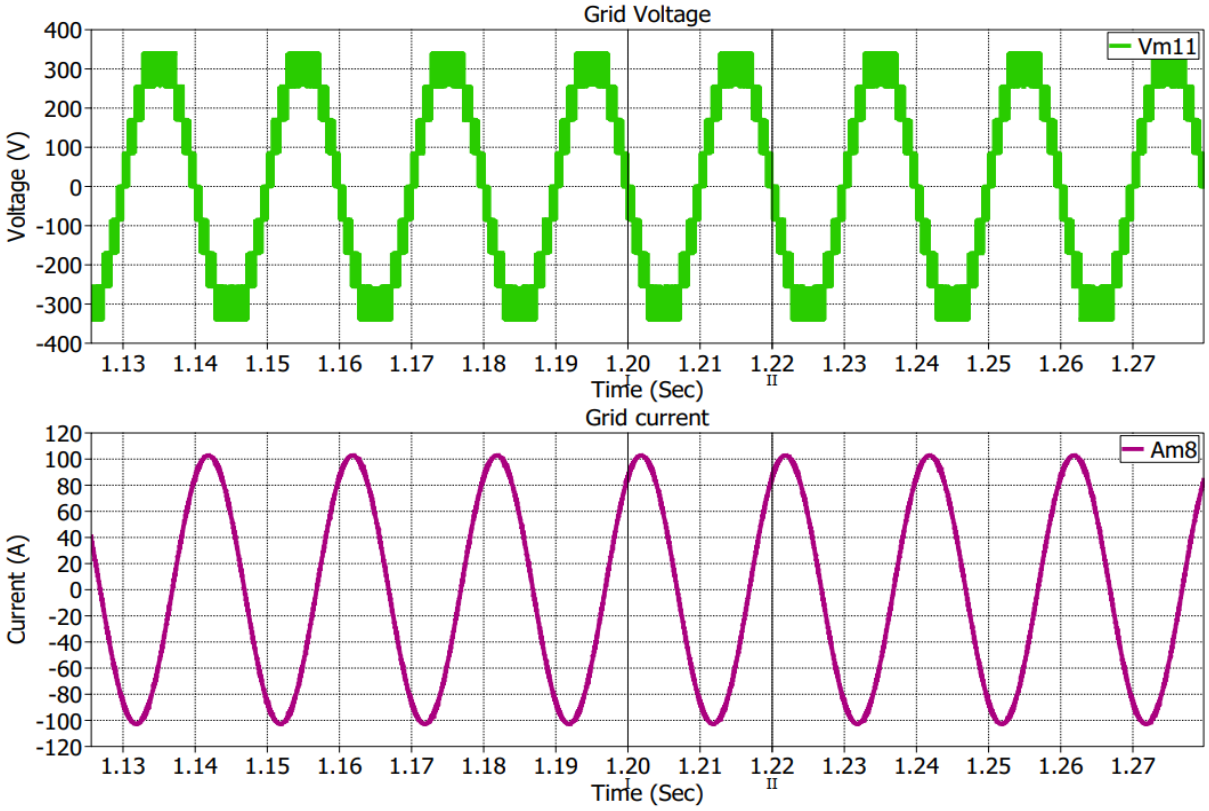

Figure 10. Three phase voltage and Current wave form

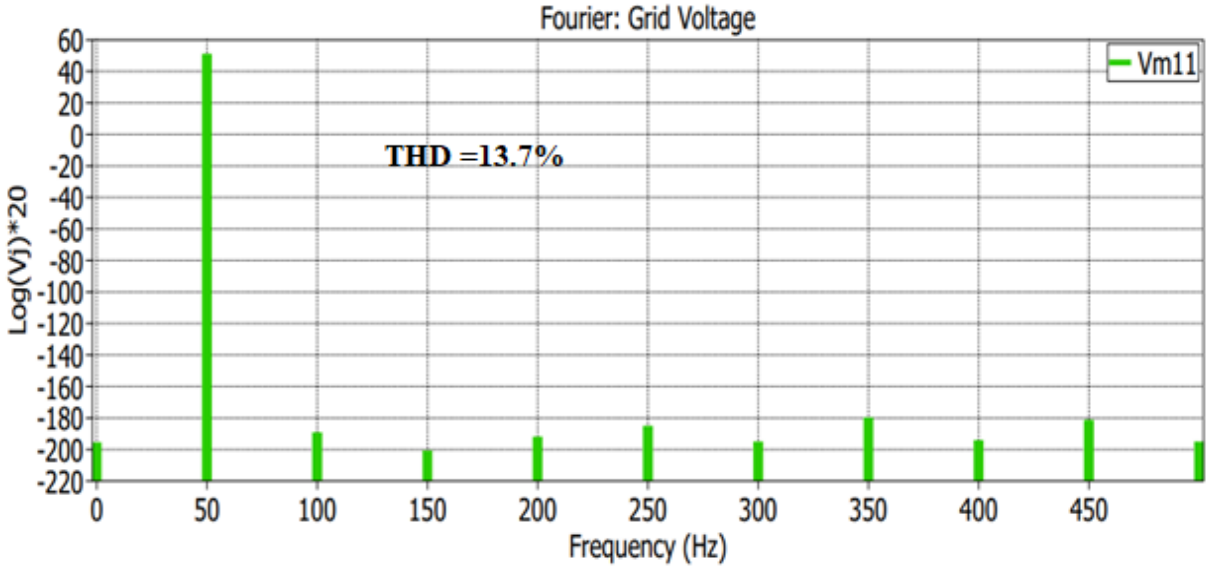

Figure 11. Fourier spectrum of phase voltages for N= 10 (N refers to integer multiplying base frequency)

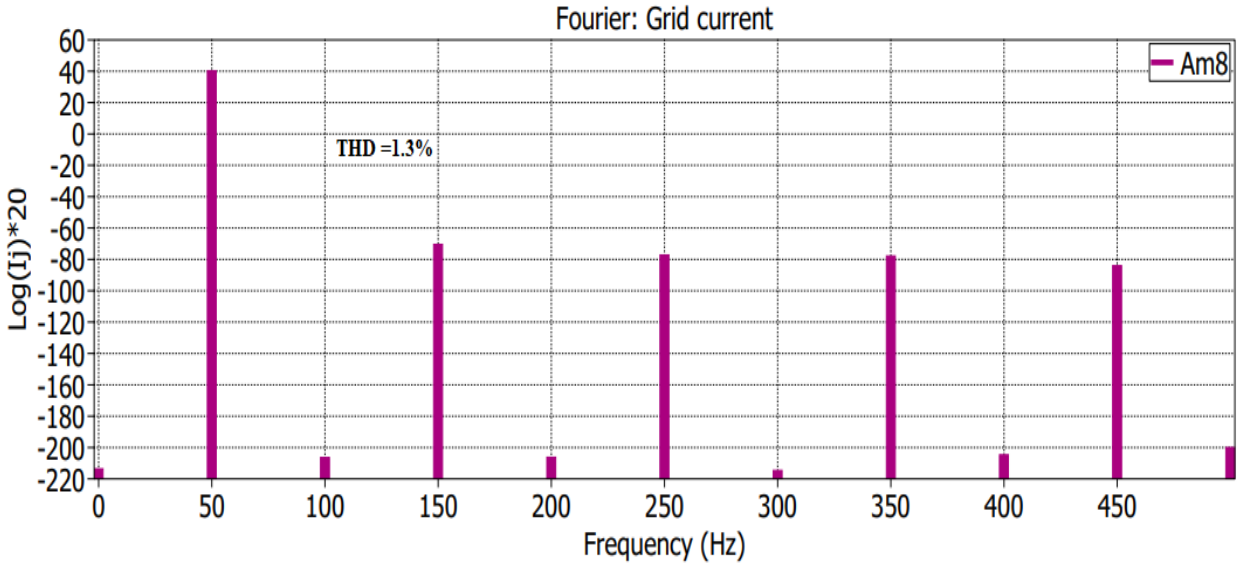

Figure 12. Fourier spectrum of phase currents for N=10

As shown from Figure 10 to Figure 12, CHB-based BEC yields a nine-level output voltage with a THD value of 13.7%, while its load current for R-L loads is about 72A (RMS) with a THD value of 1.3%. The THD value for N-harmonic order is expressed as a common logarithm multiplied by 20.

A.2. Performance for load change (from 25kW to 50kW)

The demand for the load in the distribution system changes dynamically as a result of changes in daily activities. The performance of the system when demand changes from 25kW to 50kW is shown in Figure 13 below:

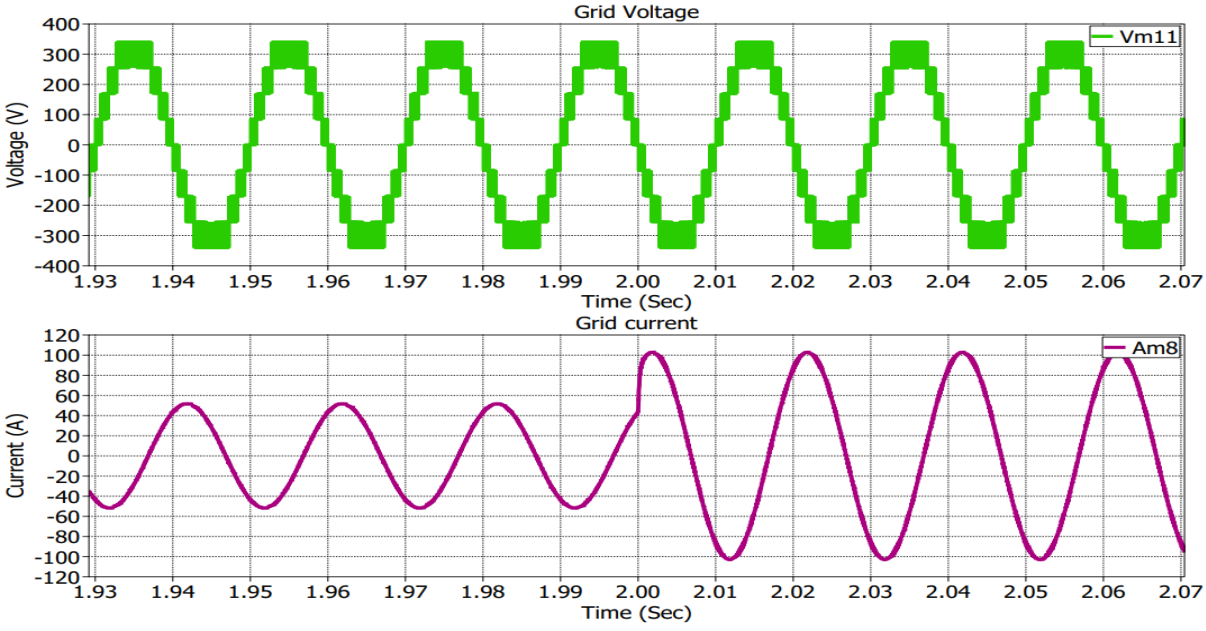

Figure 13. Performance for Load change

Journal of Science and Inclusive Development Vol. 5, No. 2, DOI:10.20372/jsid/2023-256

As shown in Figure 13, when load demand steps from 25kW to 50kW, the current demand is doubled while there is no change in the voltage magnitude.

A.3. Performance for changes in carrier frequency and modulation index

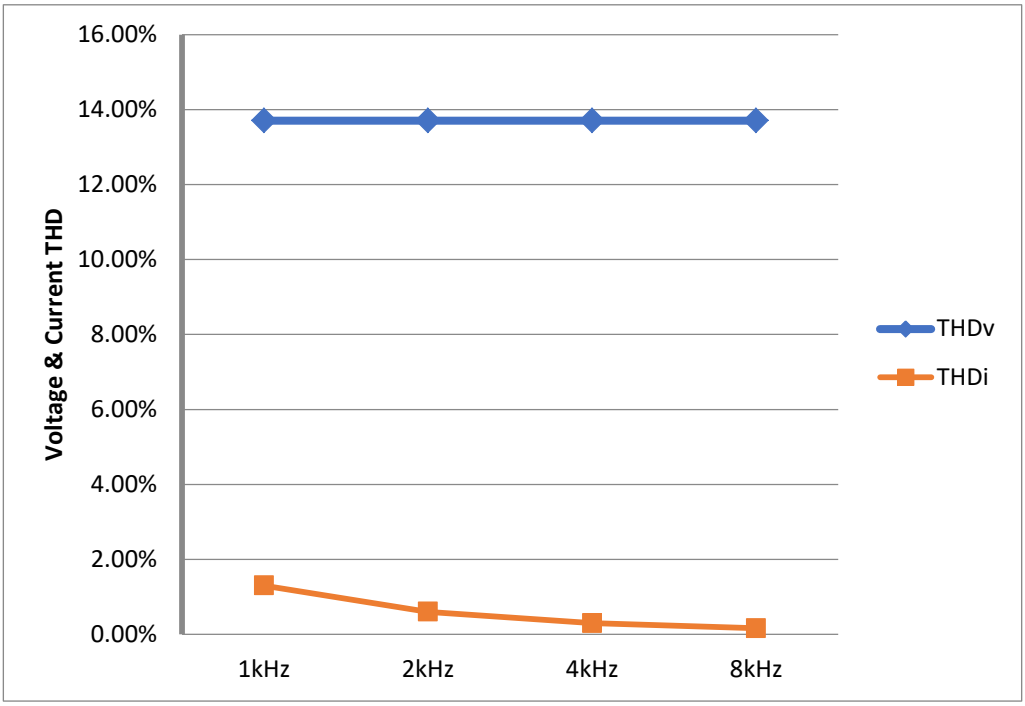

Figure 14. Changes in THD as function of carrier frequency

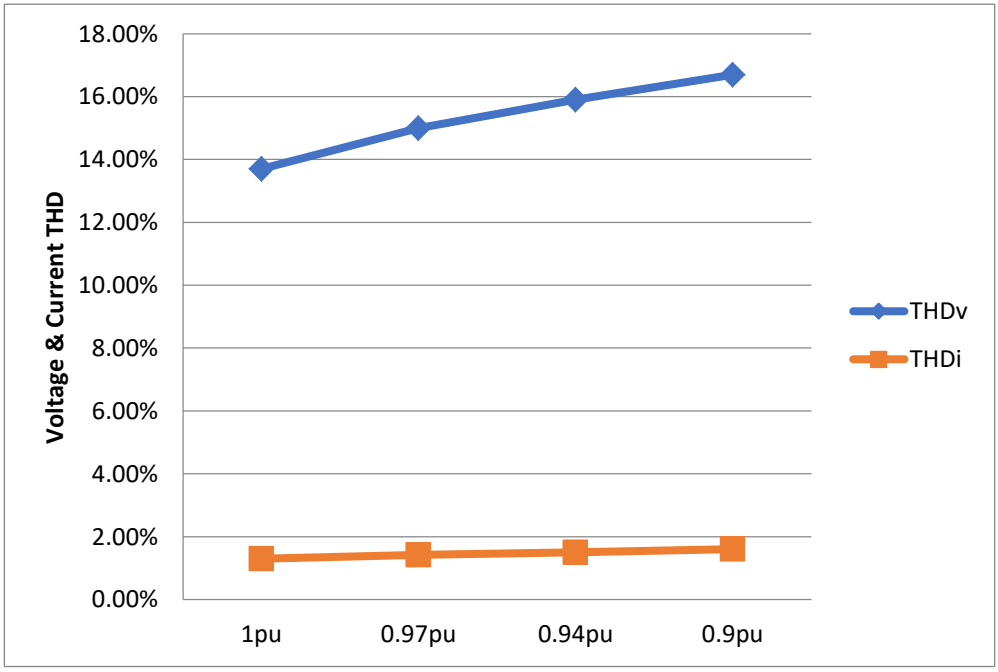

Figure 15. Changes in THD as function of modulation index

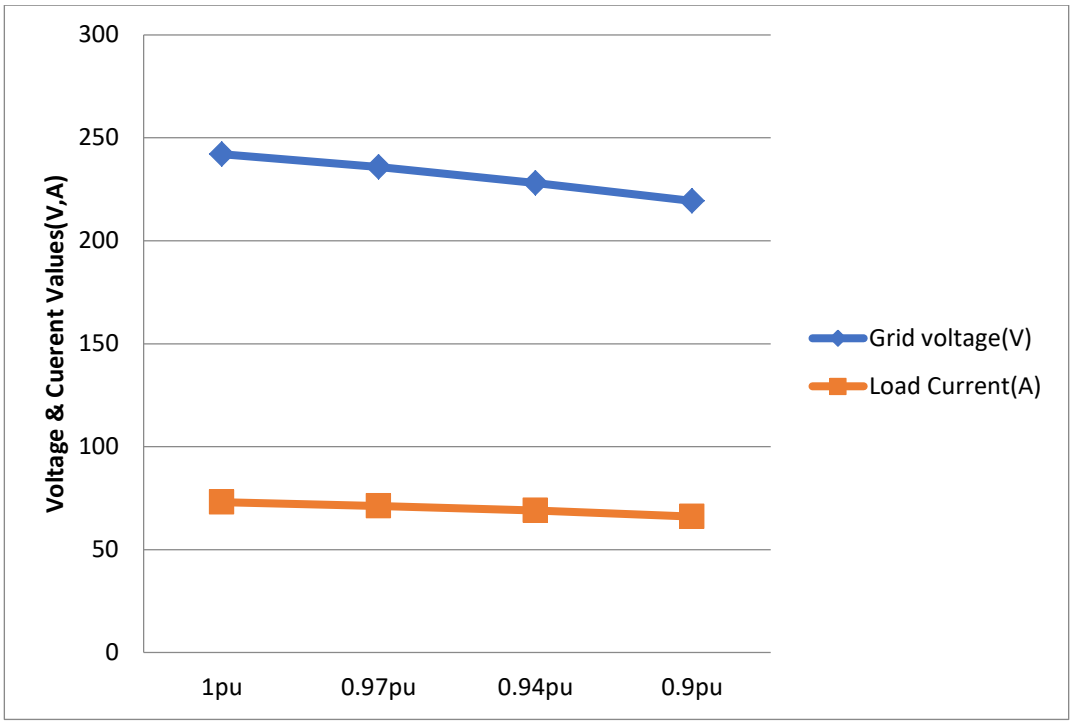

Figure 16. Changes in Voltage & Current magnitude as a function of modulation index

The results indicated (see Figures 14 to 16) that an increase in carrier frequency from 1 kHz to 8 kHz causes a decrease in the current THD values while the voltage THD value is not affected. The reason is that as carrier frequency increases, the dominant odd and triplen frequency spectrum of unwanted harmonics shifts towards higher frequencies. The decrease in modulation index (Mi) from 1 to 0.9 resulted in a substantial increase in the voltage THD value, while the increase in the current THD value was small. The cause for this is that as the modulation index decreases, the dominant frequency spectrum of unwanted harmonics is shifted towards lower frequencies. The Decrease in modulation index from 1 to 0.9 decreases the magnitudes of both voltage and current, as the modulation index and magnitude of output voltage are linearly related. Both carrier frequency and modulation index have an impact on the THD factor of the inverter output voltage.

Journal of Science and Inclusive Development Vol. 5, No. 2, DOI:10.20372/jsid/2023-256

B) Result for MMC based BEC

B.1. Output voltage and current for R-L load

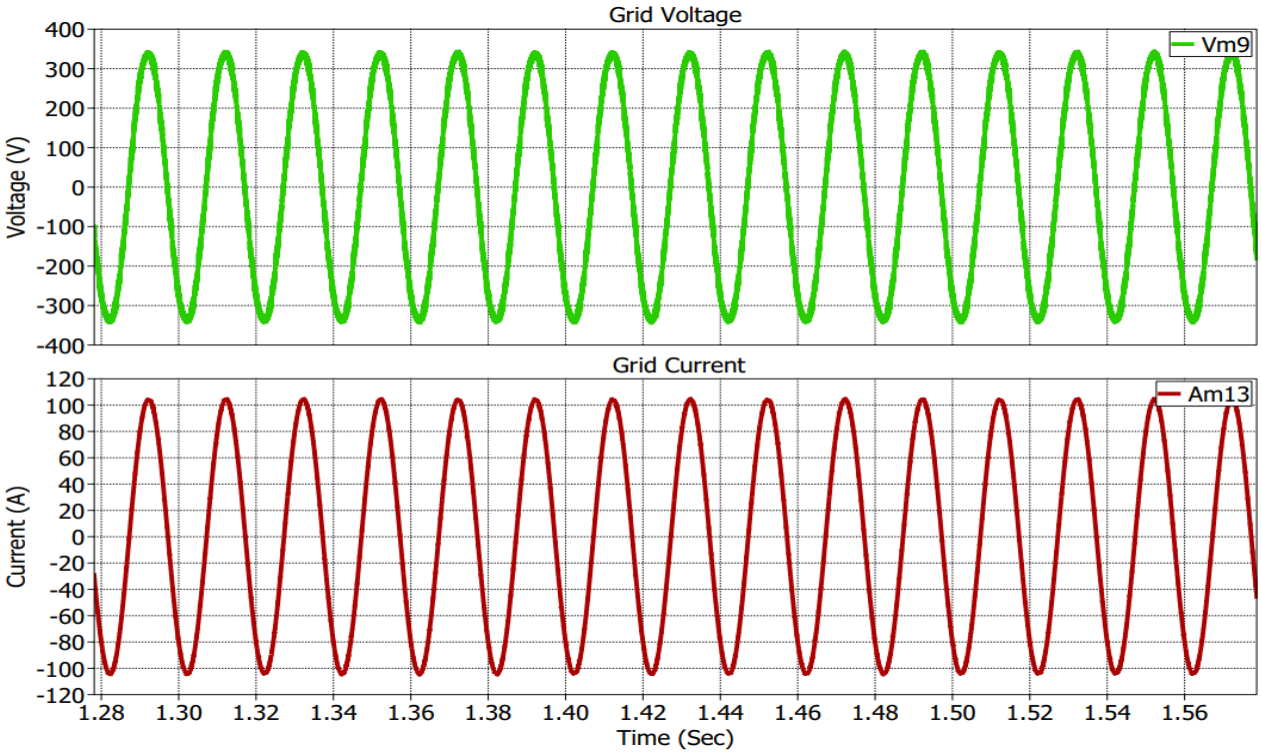

Figure 17. AC Voltage and Current Wave form of BEC based on MMC

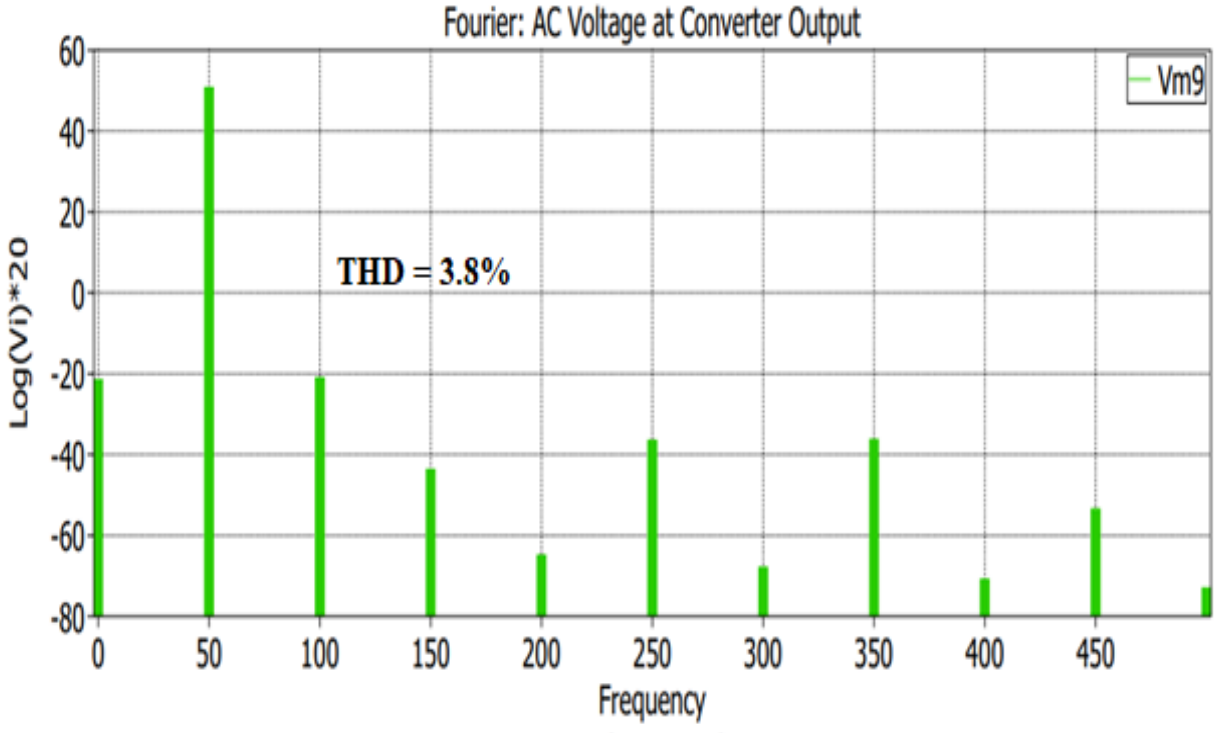

Figure 18. Fourier Spectrum of AC voltage of BEC based on MMC

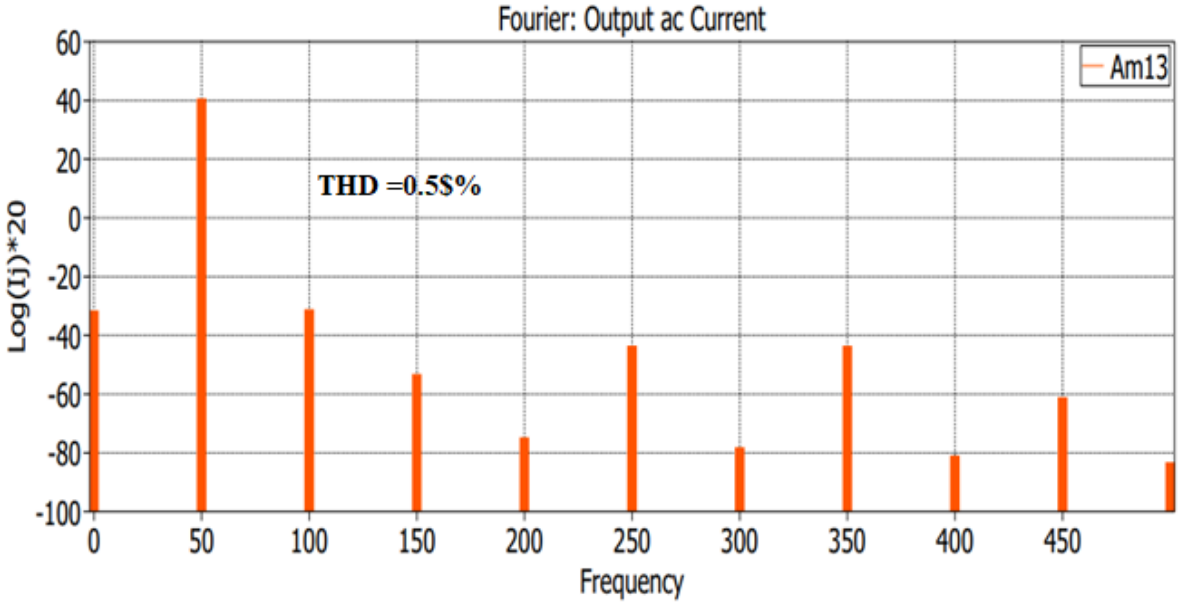

Figure19. Fourier Spectrum of load current of BEC based on MMC

As shown from Figure 17 to Figure 19, MMC-based BEC yields output voltage and current with lower THD values of 3.8% and 0.5%, respectively, for the same R-L load

C. Efficiency analysis for Converter made from chosen SM types

For efficiency analysis, the two selected silicon carbide power MOSFETs are chosen as building blocks for CHB and MMC converters. The efficiency analysis is done by using a combination of a look-up table and a formula for maximum load current and a case temperature of 1000C. All thermal parameters are gathered from the device manufacturer's datasheet (Wolfspeed, 2022; ROHM, 2018). Switching loss, conduction loss, and total semiconductor loss of the converter containing 48 power switches made of the selected semiconductor switch types are obtained by using the efficiency calculation model presented in Figure 8. The converter system efficiency, as shown in the model, is calculated as follows:

$$\eta = \frac{P_{out}}{P_{in}} \qquad (22)$$

$$\eta = \frac{P_{in} - P_{loss}}{P_{in}} \qquad (23)$$

Dividing the numerator and denominator of equation (21) by P_{in} gives the following expression for efficiency:

$$\eta = 1 - \frac{P_{loss}}{P_{in}} \qquad (24)$$

Journal of Science and Inclusive Development Vol. 5, No. 2, DOI:10.20372/jsid/2023-256

Where P_{loss} is total loss in the converter obtained by summing up switching and conduction losses, and P_{in} is the input power obtained by product of input DC voltage and current.

The overall losses and efficiency of the MMC based converter is presented in Table.3 below.

Table 3. Semiconductor losses

Device Name	Switching Loss(W)	Conduction Loss (W)	Total Loss (W)	Efficiency (%)
SiC MOSFET (SCT3017AL)	1029.54	818.69	1848.23	96.63
SiC MOSFET (C3M0015065D)	6987.3	390.9	7378.2	86.53

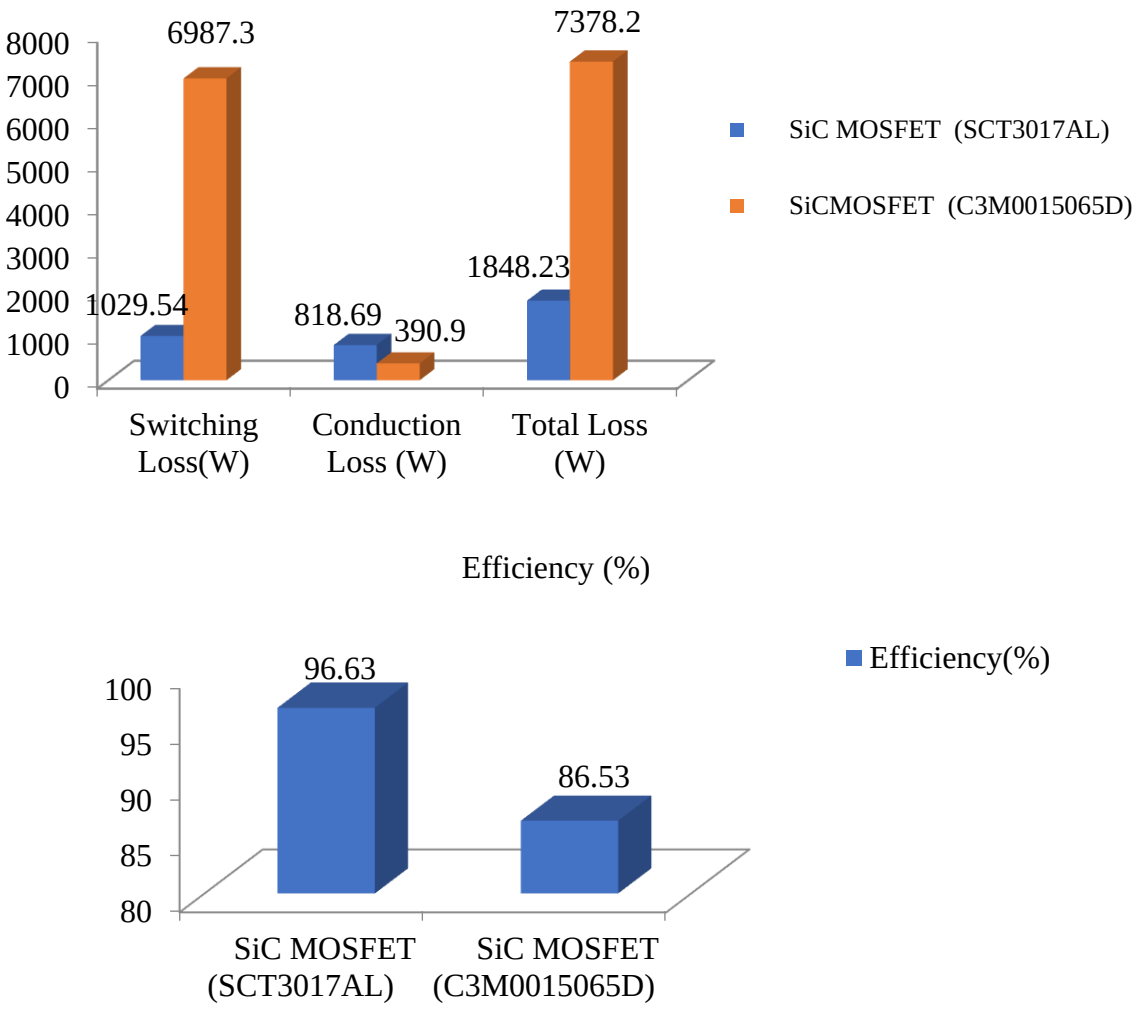

Figure 20. Switching and conduction losses

D. Performance comparison of CHB & MMC based modular converter

Table 4 shown below describes the comparisons of performance parameters of CHB and MMC-based BEC for the same load type (R-L load) and the same modulation index, frequency, and thermal model of sub-module

Table 4. Comparative performance analysis

Converter Topology	Voltage THD (%)	Current THD (%)	SM Current Stress (A)	Efficiency (%)
CHB based BEC	13.7	1.6	72	83
MMC based BEC	3.8	0.33	45(61%)	96.63

In comparison with the IEEE 519-1992 bench mark, results illustrated (see Table 5) that modular converters based on MMC have better and acceptable performance (THD value) than CHB-based converters for the same load type. Moreover, an MMC-based modular converter has less sub-module (SM) RMS current stress (61% in CHB) because of the total load current sharing between the upper and lower sub-modules in MMC, as shown in Figure 22 below.

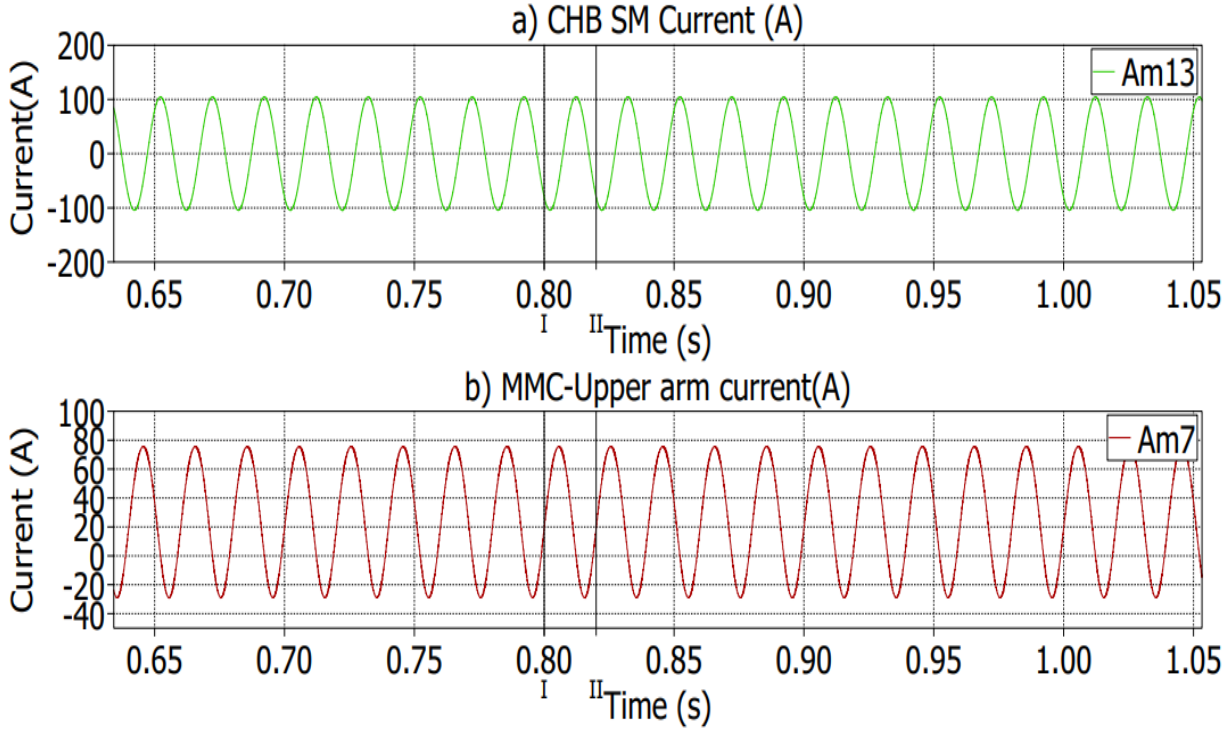

Figure 22. Sub-module current in CHB and MMC based inverter

As a result, the MMC-based converter has better efficiency for the same sub-module type (SCT3017AL) than the CHB-based converter.

Conclusion

This research compares the performance of CHB and MMC-based back-end converters (BEC) of smart transformers for a 415V, 50Hz distribution network with 50kVA system loads. Four full bridge sub-modules (FBSM) are used to construct a CHB-based BEC, and four half bridge sub-modules (HBSM) per leg arm are used to model an MMC-based BEC. Phase shift PWM with carrier frequencies ranging from 1 kHz to 4 kHz and a modulation index of 1 to 0.9 was used. Simulation results show that for the same modulation index, load type, and number of modules, MMC-based BEC has lower voltage and current THD, higher system efficiency than CHB-based BEC. As the carrier frequency goes up, the THD of the current goes down, but the THD of the voltage stays the same. For a decrease in modulation index (Mi), both voltage and current THD were increased. The sub-module in a CHB-based modular converter is exposed to higher current stress than that in a MMC based modular converter. The magnitude of grid-side voltage and load current decreases as the modulation index decreases. Semiconductor loss analysis showed that switching loss is greater than conduction loss for both selected switches (Figure 20). From the two chosen power semiconductor switches, the SiC MOSFET (SCT3017AL) has a good efficiency of 96.63% (see Figure 21).

Acknowledgment

The authors want to thank Adama Science and Technology University and Arba Minch University for their technical and financial help during the research work and preparation of the manuscript. Our heartfelt thanks also go to Plexim Company for giving us a license for PLECS software.

Declaration of conflicts of interest

The authors declare that they have no conflicts of interest regarding this research work.

Data availability

The data used in the research work were obtained from device manufacturers and are available from the corresponding author upon request.

References

Arvind Balachandran. 2019. Performance evaluation of modular multilevel converters for photovoltaic systems. MSc Theis. Linköping University, Sweden.

Costa LF, Hoffmann F, Buticchi G, Liserre M. 2017. Comparative analysis of MAB dc-dc converters configurations in modular smart transformer. IEEE, 8th International Symposium on Power Electronics for Distributed Generation Systems (PEDG), Florianopolis.

Hannan MA, Pin Jern Ker, Hossain Lipu MS, Zhen Hang Choi, Safwan ARM. et al. 2020. State of the art of Solid-State Transformers: Advanced topologies, implementation issues, recent progress and improvements. IEEE Access. 8:19113-19132

Hrishikesan VM, Anup Kumar Deka, Chandan Kumar. 2020. Capacity enhancement of a radial distribution grid using smart transformer. IEEE Access. 8: 72411- 72423.

Jayakuma M, Vanitha V. 2019. Performance analysis of different level Modular Multilevel Converters. IEEE International Conference on Electrical, Computer and Communication Technologies (ICECCT), Coimbatore, India.

Konstantinou G, Pou J, Ceballos S, Darus R, Agelidis VG. 2016. Switching frequency analysis of staircase-modulated modular multilevel converters and equivalent PWM techniques. IEEE Trans Power Deliv. 31(1):28-36.

Kumar C, Zhu R, Liserre M. 2017. Investigation of load compensation features of smart transformer in medium voltage grid. IECON 2017 - 43rd Annual Conference of the IEEE Industrial Electronics Society, Beijing.

Marcelo A. Perez, Salvador Ceballos, Georgios Konstantinou, Josep Pou, Ricardo P. Aguilera. 2021. Modular Multilevel Converters: Recent achievements and challenges. IEEE open J Ind Electron Soc. doi:10.1109/OJIES.2021.3060791.

Mikkili S, Krishna, RV, Bonthagorla PK, Senjyu, T. 2022. Performance analysis of Modular Multilevel Converter with NPC Sub-Modules in Photovoltaic Grid-Integration. Appl Sci. 12, 1219.

Muhammad F, Rasheed H, Ali I, Alroobaea R, Binmahfoudh A. 2022. Design and Control of Modular Multilevel Converter for Voltage Sag mitigation. Energies 15: 1681.

Pierluigi Guerriero, Marino Coppola, Fabio Di Napoli, Gianluca Brando, Adolfo Dannier. 2016. Three-Phase PV CHB Inverter for a distributed power generation system. Appl Sci. 6: 287.

Plexim GmbH. 2023. The simulation platform for power electronic systems user manual version 4.7. http://www.plexim.com

ROHM. 2018. TSQ50211-SCT3017AL datasheet. http:// www.rhom.com

Rohner S, Bernet S, Hiller M, Sommer R. 2010. Modulation, losses and semiconductor requirements of modular multilevel converters. In IEEE Trans Ind Electron. 57(8):2633–2642.

Subhadeep Bhattacharya, Diego Mascarella, Géza Joós. 2013.Modular Multilevel Inverter: A Study for automotive applications. 26th IEEE Canadian Conference of Electrical and Computer Engineering (CCECE).

Wolfspeed. 2022. C3M0015065D datasheet http://www.wolfspeed.com/power.

Zhang Y, Adam GP, Lim TC, Finney SJ, Williams BW. 2012. Analysis of modular multilevel converter capacitor voltage balancing based on phase voltage redundant states. IET Power Electron. 5(6):726–738.